Tectonophysics 717 (2017) 127–138

Contents lists available at ScienceDirect

Tectonophysics

journal homepage: www.elsevier.com/locate/tecto

Variations of the effective elastic thickness over the Ross Sea and Transantarctic Mountains and implications for their structure and tectonics

Fei Ji [a,b,*], Jinyao Gao [b,**], Fei Li [a,**], Zhongyan Shen [b], Qiao Zhang [b], Yongdong Li [c]

[a] Chinese Antarctic Center of Surveying and Mapping, Wuhan University, Wuhan, China
[b] Second Institute of Oceanography, Key Lab of Submarine Geosciences, SOA, Hangzhou, China
[c] Institute of Geophysics and Geomatics, China University of Geosciences, Wuhan, China

ARTICLE INFO

Article history:
Received 24 November 2016
Received in revised form 12 July 2017
Accepted 15 July 2017
Available online 21 July 2017

Keywords:
Effective elastic thickness
Ross Sea
Transantarctic Mountains
Lithospheric structure
Tectonics

ABSTRACT

The effective elastic thickness (T_e) is a proxy for lithospheric strength, and it depends primarily on the thermal gradient and composition of the lithosphere. Accordingly, spatial variations in T_e reflect changes in lithospheric properties and can be used to better understand the structure and tectonics of particular regions. In this paper, we investigate the Ross Sea and Transantarctic Mountains in terms of T_e using gravity and topographic data and the fan wavelet transform technique. The results reveal that relatively high T_e values dominate in the extensional basins of the Ross Sea and the hinterland of Transantarctic Mountains, whereas very low T_e values occur along the Transantarctic Mountain Front and in the deep ocean basin, with the lowest T_e values are found the vicinity of Ross Island and onshore in northern Victoria Land. In addition, the spatial variations in T_e correlate well with lithospheric structure at the regional scale. By combining these findings with published seismic and heat flow data, we conclude that the presence of a zone of anomalously low T_e values parallel to the coast indicates that the lithosphere beneath the Transantarctic Mountain Front is extremely weak due to Cenozoic volcanism and extension. The T_e values increase from the Transantarctic Mountain Front (7 km) toward the center of the continent (~80 km), which indicates that the continental lithosphere underlying East Antarctica belongs to the classic Gondwanan craton. The increase in T_e indicates that the Transantarctic Mountain Front marks the continent-continent boundary between East Antarctica and West Antarctica. The T_e values in the other extensional basins of the Ross Sea exhibit little variation and average approximately 35 km. The relatively high T_e values are interpreted to indicate that the lithosphere cooled and became mechanically stronger between late Cretaceous extension and Eocene-Neogene deposition.

1. Introduction

The Transantarctic Mountains (TAM), one of the largest mountain ranges in the world, and adjacent East Antarctica are covered by thick perennial ice, which makes it almost impossible to conduct direct and extensive observations. The nearby Ross Sea is an extensive area of open water that connects the Southern Ocean and the West Antarctic Rift System (WARS) and has become a major focus of research, due to the distinctive multi-phase tectonic activity that has occurred in this region since the beginning of extension in the late Cretaceous. This activity has featured events such as the uplift of the TAM, right-lateral strike-slip motion in northern Victoria Land and rifting and magmatism in the western Ross Sea (Cande et al., 2000; Cooper et al., 1987; Salvini et al., 1997). Although several studies (Karner et al., 2005; Lawrence et al., 2006a; Salvini et al., 1997; Stern and ten Brink, 1989; Trey et al., 1999) have been conducted in this study region, e.g., ANTOSTRAT (Cooper et al., 1987), ACRUP (Trey et al., 1999) and TAMSEIS (Lawrence et al., 2006a), only limited information exists on the mechanical properties and deformation of the lithosphere and the relationships between these factors and tectonics.

Mechanical strength is a lithospheric property that is fundamental in controlling the deformation processes that occur in response to long-term ($>10^5$ years) geological loads (Burov and Diament, 1995). It can be described in terms of the effective elastic thickness (T_e) or the flexural rigidity (D) (Watts, 1978). The relationship between these two parameters can be expressed as $D = ET_e^3/[12(1-\nu^2)]$, where E (Young's modulus) and ν (Poisson's ratio) are treated as constants in this paper.

* Correspondence to: F. Ji, Chinese Antarctic Center of Surveying and Mapping, Wuhan University, Wuhan, China.
** Corresponding authors.
E-mail addresses: jifeii@163.com (F. Ji), jygao@mail.hz.zj.cn (J. Gao), fli@whu.edu.cn (F. Li).

http://dx.doi.org/10.1016/j.tecto.2017.07.011
0040-1951/

As an alternative measure of lithospheric strength, T_e corresponds to the thickness of an imaginary elastic thin plate overlying an inviscid substrate that bends to a degree equal to that of the real lithosphere under the same applied load (Pérez-Gussinyé et al., 2004; Tassara et al., 2007). The values and meanings of the T_e for continents differ from those for oceanic plates (Watts and Burov, 2003). The T_e of oceanic lithosphere is a function of the lithospheric age at the time of loading (Bodine et al., 1981; Watts, 1978) and is generally equal to the depth of the 450 °C isotherm (Watts and Fairhead, 1999). The corresponding values are normally <50 km. For continents, however, many properties control the value of T_e, particularly the composition, structure and thermal gradient of the lithosphere and the degree of decoupling between the crust and the mantle (Burov and Diament, 1995). Consequently, the T_e of continental lithosphere varies a greater degree than that of oceanic lithosphere. Several studies have shown that T_e values are very large in old lithosphere and may exceed 100 km in areas such as in the Canadian Shield and South American cratons (Kirby and Swain, 2014; Pérez-Gussinyé et al., 2009; Tassara et al., 2007). In contrast, volcanic provinces and rift valleys within continental lithosphere are characterized by low T_e values. Additionally, the relationships between T_e and surface heat flow, seismic velocity and seismogenic layer thickness have been previously investigated and discussed (Mao et al., 2012; Pérez-Gussinyé et al., 2007; Watts and Burov, 2003).

In the last several decades, different methods have been carried out to estimate T_e in different regions. Dorman and Lewis (1970) developed the linear response function technique to study isostasy using topography and gravity anomalies, and the spectral analysis method was subsequently introduced to estimate T_e. The recovered T_e values develop from results for a single specific study targets, e.g., seamounts (Watts, 1978; Watts et al., 1975) to spatial variations of T_e that reflect different tectonic regimes (Chen et al., 2013; Ratheesh Kumar and Windley, 2013). This contributes significantly in the efficient analysis of lithosphere structure in entire study area with T_e variations. Forsyth (1985) found that, if internal loads were ignored, the T_e values would be underestimated, and suggested that both the surface and internal initial loads should be considered in the flexure models. In addition, although some approaches provide maps of T_e variations, an averaged T_e is estimated in an analysis window with fixed size, which is also likely to affect the estimated T_e (Pérez-Gussinyé et al., 2004). Thus, Kirby and Swain (2004, 2011) introduced the fan wavelet coherence method that address the issues described above and provides a robust way to estimate T_e.

Over the past three decades, several methods (Cande et al., 2000; Karner et al., 2005; Lawrence et al., 2006b; Stern and ten Brink, 1989;) that are based on thermal evolution, plate reconstructions and flexural models, have been proposed to explain the mechanisms of lithospheric deformation and the geodynamical features of the Ross Sea and TAM. However, some questions remain debatable or unresolved. (I) Uplift of the TAM may have been linked with episodic extension in the Ross Sea, but what was the uplift mechanism? (II) What is the nature of the lithospheric deformation and mechanical strength underlying the Ross Sea and the relationship between these factors and tectonic conditions? (III) Where is the tectonic boundary between the Mesozoic and Cenozoic terranes?

In this paper, we concentrate on these unresolved questions. Here, we present new high-resolution T_e maps covering the TAM, the Ross Sea and the surrounding areas that were obtained by applying the fan wavelet coherence technique to satellite-terrestrial gravity model and topography. First, the geologic setting of the study area is described. We then describe the dataset and methods used, as well as the recovered spatial variations in T_e. We then compare our results with previous related studies and examine the relationship between the results and surface heat flow estimates. Finally, we discuss the implications of the T_e values for the interpretation of lithospheric deformation and tectonic activity in the Ross Sea and the TAM.

2. Geologic setting

Antarctica can be divided into three primary tectonic regions, East Antarctica, the WARS and the TAM, which delineate the boundary between the WARS and East Antarctica (Fig. 1). The study region, which is located at the end of the WARS, consists of the TAM, the extensional basins in the Ross Sea and the surrounding areas. According to the seismic data recorded by the TAMSEIS project, which investigated the crustal structure beneath the TAM and the adjacent area, the crustal thickness of the East Antarctic craton averages 35 km and varies little. In contrast, the Ross Sea features thinned crust that is only approximately 20 km thick (Lawrence et al., 2006a). The timing of the formation of East Antarctica is controversial, but most studies suggest that the assembly of the craton occurred during the Precambrian (Fitzsimons, 2003; Grikurov, 1982). The TAM extends >3000 km across the continent from northern Victoria Land to the Weddell Sea, and individual peaks reach heights of 4500 m above sea level (Robinson and Splettstoesser, 1984). The main phase of uplift began at 55 Ma (Fitzgerald, 1994, 1992). The Moho depth profiles obtained from receiver function analysis show that the Moho deepens from inland toward the TAM and reaches about 40 ± 2 km at 100–200 km away from the coast (Agostinetti et al., 2005; Lawrence et al., 2006a). An et al. (2015) published a Moho depth map that was based on the constructed 3D shear velocity model and the results show that the Moho beneath the TAM is deeper in the south and occurs at depths of up to 44 km at a latitude of approximately 85°S. Hansen et al. (2016) found that the Moho depth is 46 ± 4 km under the northern TAM, based on the new seismic data from the Transantarctic Mountains Northern Network (TAMNNET). Because the TAM represent the largest noncontractional mountain belt and the highest continental rift-flank uplift on Earth (Stern and ten Brink, 1989; Sugden and Denton, 2004), the cause of the uplift has been a hot research topic. Broadly, the uplift has been attributed to flexural uplift of the mountains (Stern and ten Brink, 1989; ten Brink and Stern, 1992), thermal effect (Smith and Drewry, 1984) and a combination of both (ten Brink et al., 1997). Earlier studies of flexural models assumed that a deep normal fault had broken the plate and the formation of the TAM is associated with uplift at the end of broken plate, between East and West Antarctica. Even though there is no geophysical evidence that supports the presence of a penetrating fault (ten Brink et al., 1993), the significant differences in thickness and temperature of lithosphere between East and West Antarctica have resulted in local deformation of the lithosphere and the development of a deeply border normal fault at the transition. Consequently, recent studies of uplift of the TAM based on numerical models still consider the broken plate as a key factor in the flexural model (Yamasaki et al., 2008). Smith and Drewry (1984) suggest the anomalously hot asthenosphere, which was later identified from seismic data (Hansen et al., 2016; Lawrence et al., 2006b), penetrated into the lithosphere, causing the separation of the plates that aided in the uplift of the TAM. Lawrence et al. (2006a) argued that part of the uplift of the TAM is the consequence of the flexure related to a buoyant thermal load. This hypothesis is currently one of most important viewpoints regarding the uplift of the TAM.

The Wilkes Subglacial Basin (WSB) (Fig. 5), which extends 1400 km long and 600 km wide, is hidden beneath thick ice in the East Antarctica (Ferraccioli et al., 2009). Based on the aeromagnetic, airborne radar and gravity data, the WSB is interpreted as a major sedimentary basin covered by low-density sediments that are <1 km thick (Drewry, 1976; Ferraccioli et al., 2009; Studinger et al., 2004). These studies suggest that the WSB may be a rift basin with thinned continental crust. Other studies based on receiver functions, airborne gravity data (Hansen et al., 2016; Jordan et al., 2013) suggest that the Moho depth in the WSB decreases by about 5 km from southeast to northwest across the WSB (see the arrow in Fig. 5). Jordan et al. (2013) argue that the thinned crust in the WSB may be related to Mesozoic extension, Cenozoic glacial erosion and other processes.

To the east of the TAM, the Ross Sea is a broad submerged region that is distinctly different from East Antarctica and the TAM and features

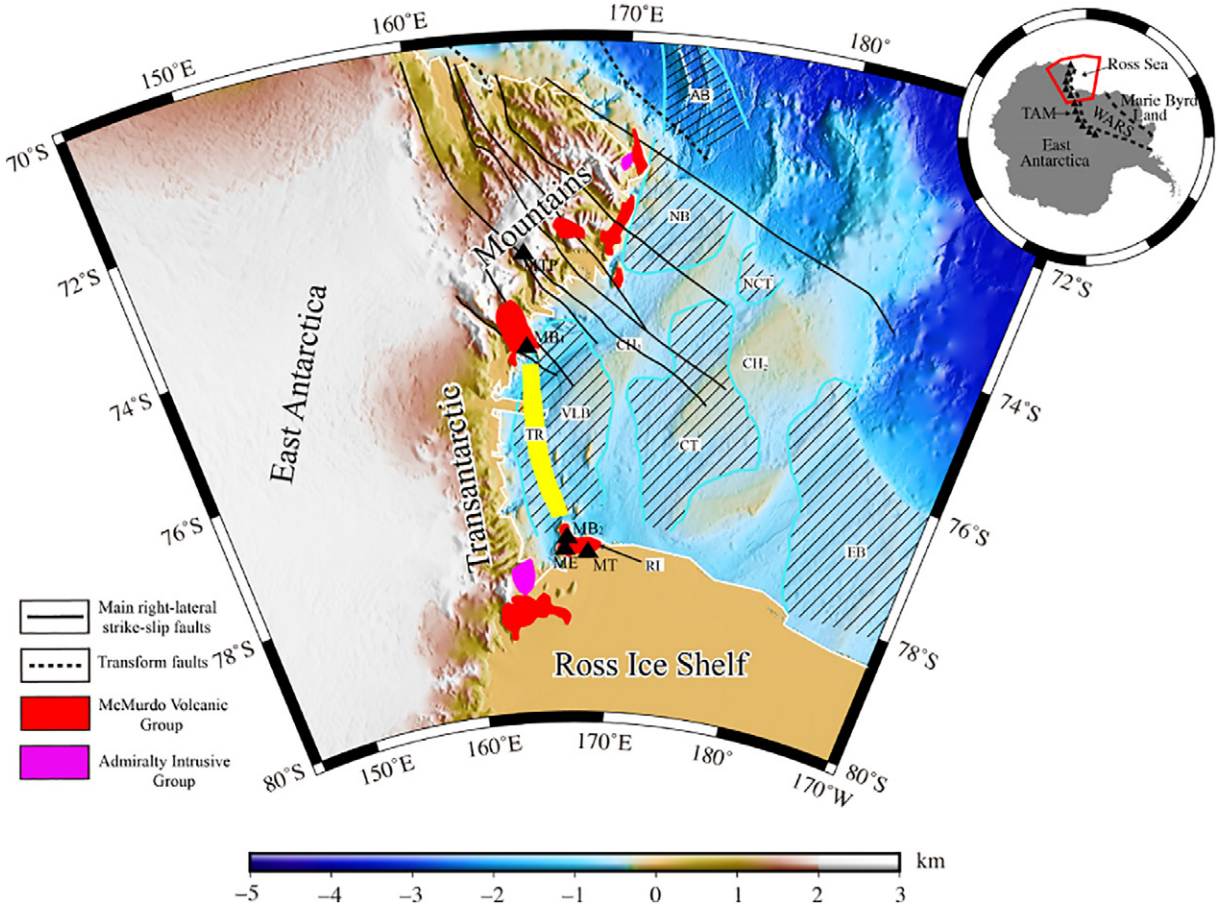

Fig. 1. Topography/bathymetry of the Ross Sea, the TAM and adjacent areas. The white line represents the coastline of Victoria Land. The major right-lateral strike-slip faults (black solid lines) are redrawn from Salvini et al. (1997). Abbreviations: AB, Adare Basin; CH_1, Central High; CH_2, Coulman High; CT, Central Trough; EB, Eastern Bain; NB, Northern Basin; NCT, Northern Central Trough; RI, Ross Island; TR, Terror Rift; VLB, Victoria Land Basin. The black triangles show the locations of volcanoes. Abbreviations: MB_1, Mt. Melbourne; MB_2 Mt. Bird; ME, Mt. Erebus; MT, Mt. Terror; MTP, Mt. The Pleiades.

highly stretched crust, thick sediments and high heat flow (Blackman et al., 1987). At continental margin, the beta factor, which was proposed by McKenzie (1978), is equal to initial crustal thickness before stretching divided by the post-rift crustal thickness. The OBS profile acquired by the ACRUP project reveals that the beta factor varies between 1.6 and 4.0 within the Ross Sea, suggesting that the crust there is highly stretched (Trey et al., 1999). The results of seismic reflection surveys show that the extensional basins in the Ross Sea are covered by thick sediments that reach 14 km in Victoria Basin (Cooper et al., 1987). Several active volcanoes are located in the western Ross Sea, such as Mt. Erebus and Mt. Melbourne (Fig. 1), indicating the presence of a thermal anomaly in the upper mantle. A low-velocity anomaly has been detected in the upper mantle beneath Ross Island using seismic tomography (Watson et al., 2006). Additionally, Lawrence et al. (2006b) found that the Ross Sea has a hotter and less dense mantle compared with East Antarctica.

The Ross Sea formed during two distinct phases of extensional activity. The first phase occurred in the late Cretaceous and was characterized by several hundred kilometers of extension within the Ross Sea (Behrendt et al., 1991; Fitzgerald et al., 1986). The regional intracontinental extension in the Mesozoic led to the thinning of the crust and the formation of three mainly N-S-trending sedimentary basins in the Ross Sea, the Victoria Land Basin, the Central Trough and the Eastern Basin (Fig. 1). The second phase of extension began since Paleogene time and has continued episodically to the present (Hall et al., 2007; Salvini et al., 1997). According to the distribution of abundant Cenozoic volcanism and tectonism, the later extensional event is not as broadly distributed as the first phase and is only locally distributed in the western Ross Sea. Evidence provided by plate reconstruction suggests that approximately 180 km of extension occurred in the western Ross Sea in Eocene and Oligocene time (Cande et al., 2000). The Adare Basin, located northwest of the Ross Sea, formed along one arm of a ridge-ridge-ridge triple junction that was active between chrons C20 and C9 (43–26 Ma) (Cande and Kent, 1995). The Northern Basin is located in the continental shelf adjacent to the Adare Basin and close to the margin of Victoria Land. Continuous sedimentary sequences identified based on multi-channel seismic and magnetic anomaly data (Cande and Stock, 2006; Damaske et al., 2007) spread across the shelf break into the Northern Basin from the Adare Basin, which implies a possible linkage between the Adare seafloor spreading and the extensional tectonics of the western Ross Sea in the Neogene.

Driven by the active transform faults of the Southern Ocean, massive active right-lateral strike-slip faults extend from northern Victoria Land to the Central High in the Ross Sea. These faults reshaped the Cenozoic tectonic framework of Victoria Land and the Ross Sea (Salvini et al., 1997). Fieldwork in northern Victoria Land (Storti et al., 2001) has demonstrated that the roughly parallel right-lateral strike-slip intraplate fault systems have caused large-scale lithospheric deformation, including displacement and the development of a transtensional splay zone.

3. Data and methodology

3.1. Data

Bathymetric/topographic and Bouguer gravity anomaly are used in the coherence analysis to estimate the spatial variations in T_e in the study region. The bathymetry/topography model is derived from

ETOPO1 (Fig. 1) (Amante and Eakins, 2009). Because the coverage of shipborne gravity data is limited, we employ free-air gravity anomaly derived from the gravity model EIGEN6C3stat (Fig. 2a), with a resolution of up to degree and order 1949. This gravity model combines GRACE, GOCE and LAGEOS data plus Terrestrial (land and sea) data (Förste et al., 2012). To obtain the Bouguer anomaly (Fig. 2b), the gravity effect of ice and subglacial bedrock on the continent and that of seawater in the ocean are calculated and removed from the free-air anomaly (Gao et al., 2015). The ice-thickness model (Fig. 3a) and subglacial topography come from the recently released BEDMAP2 data product, which is a 1 km × 1 km grid dataset that covers the Antarctic and its surroundings south of 60°S (Fretwell et al., 2013). As previously noted, the topographic load should be used in estimating T_e and it is necessary to reduce the vertical density variations of the topographic load, such as those caused by sediments and seawater (ice and water in this study region) (Braitenberg et al., 2003; Wienecke et al., 2007). Here, we use the equivalent topography (Fig. 3b), referred to as model topography by Wienecke et al. (2007) as the input topography data. This process transforms the ice on the land and the seawater in the ocean into their crustal equivalents by multiplying by a factor as follows:

$$H = h_T - t_i\frac{\rho_c-\rho_i}{\rho_c}, \text{ for the land}$$

$$H = h_T\frac{\rho_c-\rho_w}{\rho_c}, \text{ for the sea, with } t_i\frac{\rho_i}{\rho_c} \text{ added if ice exists} \quad (1)$$

where H is the equivalent topography; h_T is the initial topography data; t_i is the thickness of the ice; and ρ_c, ρ_i and ρ_w are the assumed densities of the crust, ice and seawater, respectively. The values used in the calculation are shown in Table 1.

3.2. Fan wavelet coherence technique

The Bouguer coherence technique, which is based on the model of a thin uniform elastic plate above an inviscid fluid, is used to obtain the spatial variations in T_e by estimating the coherence of topography and Bouguer gravity anomaly as a function of wavelength (Forsyth, 1985). The analysis of theoretical coherence (Watts, 2001) indicates that an elastic plate will exhibit Airy isostasy and fully compensate for long-wavelength loads (>1000 km); in such situations, the coherence value is one. On the other hand, the loads are completely supported by the plate for short-wavelength loads (<50 km), for which the coherence value is zero. Consequently, the specific wavelength band referred to as the "transition wavelength" is critical, and it is the basis for subsequently recovering T_e. Forsyth (1985) showed that the initial loads include surface loads (those on top of the lithosphere) and subsurface loads (those occurring at the Moho). In the calculation, information on the depth of the Moho and the corresponding variations in interface density differences have been derived from CRUST 1.0 (Laske et al., 2013).

As Swain and Kirby (2003) pointed out, the finite window size of the Fourier Transform will bias the estimated T_e. Here we adopt the Continuous Wavelet Transform (CWT) to estimate the T_e values. The CWT involves sampling all the data in the study area at all scales at once with scaled wavelets, which produces local spectral characteristics at each data point (Kirby and Swain, 2008). Thus, the fan wavelet technique is employed to estimate T_e across the study region. The fan wavelet (Kirby and Swain, 2004) is the superposition of 2D Morlet wavelets in a 'fan-shaped' geometry based on averaging a series of 2D Morlet wavelets over a finite number of directions (Kirby, 2005).

The CWT is more easily computed in the wavenumber domain with the fast Fourier transform. For a 2D signal $g(\mathbf{x})$ in the spatial domain, its wavelet coefficients can be expressed as the inverse FFT ($\boldsymbol{F}^{-1}$) of the product of the signal with the complex conjugate of a wavelet:

$$g\sim(s,\mathbf{x},\theta) = \boldsymbol{F}^{-1}\left[G(\boldsymbol{k})\hat{\psi}^{*}_{s\theta}(\boldsymbol{k})\right] \quad (2)$$

where s and θ are the parameters associated with the scale and azimuth of the wavelet, respectively. $\mathbf{x}$ represents the spatial coordinates, $\boldsymbol{k}$ is the 2D wavenumber, $G(\boldsymbol{k})$ is the Fourier transform of $g(\mathbf{x})$ and $\hat{\psi}_{s\theta}(\boldsymbol{k})$ refers to the Fourier transform of the 2D Morlet wavelet at a certain scale and azimuth.

$$\hat{\psi}_{s\theta}(\boldsymbol{k}) = e^{-|\boldsymbol{k}-\boldsymbol{k}_0|^2/2} \quad (3)$$

where θ is the resolving direction of the wavelet. $\boldsymbol{k}_0 = (|\boldsymbol{k}_0|\cos\theta, |\boldsymbol{k}_0|\sin\theta)$ is the central wavenumber and is related to the resolution of the Morlet wavelet. As Kirby and Swain (2011) pointed out that $\boldsymbol{k}_0$ is a critical parameter in the estimation of T_e and suggested that the larger central wavenumber ($|\boldsymbol{k}_0|>5$) can result in wavelet having a poor $\mathbf{x}$-resolution but high $\mathbf{k}$-resolution and more accurate T_e values. Chen et al. (2015a, 2015b) recovered T_e over the Himalayan-Tibetan orogen and the Arabian plate using different central wavenumbers and found similar trends of T_e values in large-scale region. Here, we are more concerned with the accuracy of absolute values of T_e and we set central wavenumber as $\pi\sqrt{2/ln2} \approx 5.336$.

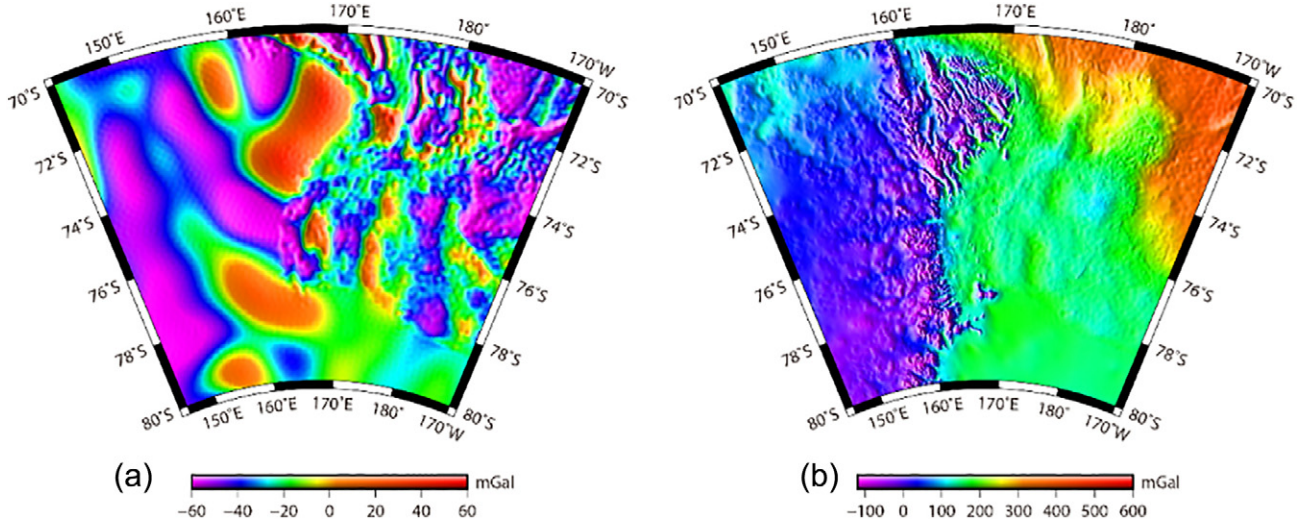

Fig. 2. Free-air gravity anomaly (a) derived from the EIGEN6C3stat model and the Bouguer gravity anomaly (b) obtained by removing the gravity effects due to the topography and the presence of the ice sheet.

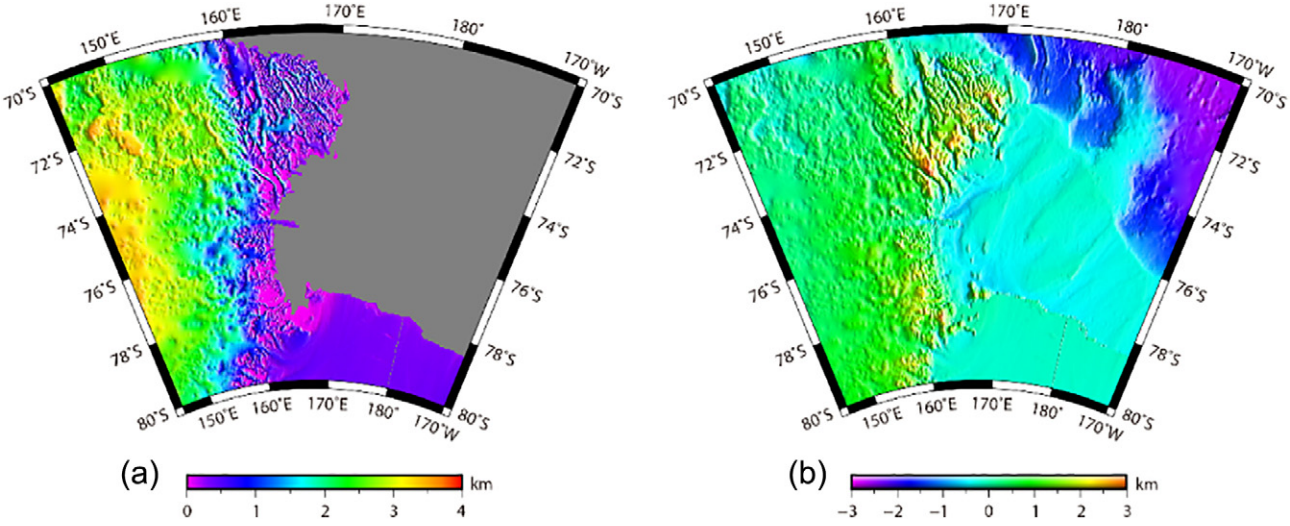

Fig. 3. Ice thickness (a) and equivalent topography (b) obtained by transforming the ice and seawater into crust.

The 2D wavelet coherence is computed by estimating the co-spectra and cross-spectra of the Bouguer gravity and topography data via

$$\gamma^2{}_{obs}(s,\mathbf{x}) = \frac{\left|g\sim_{s\mathbf{x}\theta} h\sim^{*}{}_{s\mathbf{x}\theta}\right|^2}{g\sim_{s\mathbf{x}\theta} g\sim^{*}{}_{s\mathbf{x}\theta} h\sim_{s\mathbf{x}\theta} h\sim^{*}{}_{s\mathbf{x}\theta}} \quad (4)$$

where $g\sim_{s\mathbf{x}\theta}$ and $h\sim_{s\mathbf{x}\theta}$ are the wavelet coefficients of Bouguer gravity and the topography, respectively, calculated using Eq. (2). The asterisks indicate complex conjugation, and the angular brackets represent averaging over the azimuth, which supplies isotropic coefficients if θ changes from 0° to 180° (Kirby, 2005). The coherency (Γ) is a complex variable and its relationship with coherence in Eq. (4) can be expressed as $\gamma^2 = |\Gamma|^2 = \Gamma_I{}^2 + \Gamma_R{}^2$, where the subscripts R and I indicate its real and imaginary parts, respectively. Kirby and Swain (2008) noted that, for the purpose of keeping with the traditional definition of coherence, instead of using coherence, only the square of the real part of the wavelet coherency is employed to estimate the T_e, which can reduce the error on T_e (Kirby and Swain, 2009). The imaginary part can be employed to assess the impact of noise on recovered T_e values. McKenzie (2003) showed that the "gravitational noise" due to the internal loads without topographic expression may lead to bias the estimated T_e values. To assess the noise effect, Kirby and Swain (2009) adopted the maximum value of the normalized squared imaginary part of the coherency (NSIC $\overline{\Gamma}^2{}_I = (Im\Gamma)^2/|\Gamma|^2$) between the free-air gravity anomaly and topography around the Bouguer transition wavelength to evaluate the final T_e values. If the maximum value is larger than 0.5, the T_e values in the corresponding position may be marred by the "gravitational noise" and should be excluded from the T_e analysis.

Table 1
Parameters used in the gravity correction and coherence techniques.

Parameter	Value	Units
Density of sea water	1030	$kg{\cdot}m^{-3}$
Density of crust	2800	$kg{\cdot}m^{-3}$
Density of ice	900	$kg{\cdot}m^{-3}$
Density of mantle	3300	$kg{\cdot}m^{-3}$
Young's modulus	100	GPa
Poisson's ratio	0.25	
Gravitational constant	6.67×10^{-11}	$m^3{\cdot}kg^{-1}{\cdot}s^{-2}$
Gravitational acceleration	9.80	$m{\cdot}s^{-2}$

4. Results

4.1. Spatial variations of T_e

To access the influence of "gravitational noise" in the T_e estimates, we provide the distribution of maximum values of the free-air NSIC around the transition wavelength (Kirby and Swain, 2009). The contours in Fig. 4 show the regions where T_e appears to be biased by the significant noise. Small-scale noise appears to be scattered over some parts of East Antarctica and significant noise occurs in the extensional basins of Ross Sea, e.g., in the Eastern Basin and the northern Central High. High level of noise seen in the Eastern Basin may be related to the flat topography of this area (Fig. 3b). The effects of area of low topographic variations on the distribution of noise can be found in other studies (Chen et al., 2015a; Mao et al., 2012). Despite the appearance of noise, the T_e values (Fig. 5) in the basins biased by the noise do not vary sharply compared with those in the surrounding extensional basins, suggesting that the variations of T_e correlate well with the two phases of tectonic activities in the Ross Sea. Generally, the noise affects limited areas in the study region and has no significant influence on the estimated T_e variations.

To avoid edge effects, grid data much wider than the study area have been selected and calculated to estimate the coherence between topography and the Bouguer gravity anomaly and to invert the T_e values. The distribution of T_e values ranges from 5 km to 80 km, and the values differ considerably between the oceanic lithosphere and the continental lithosphere. As shown in Fig. 5, the T_e of the Ross Sea and the TAM obtained from Bouguer coherence combined with fan wavelet analysis correlate well with tectonic boundaries and morphological structures.

In the oceanic region, including the Ross Ice Shelf, the extensional Ross Sea basins and the deep ocean basins, the T_e values are relatively low, i.e., <35 km. The lowest T_e values (<10 km) occur in front of the Transantarctic Mountain Front (TAMF) and parallel the coastline from the Adare Basin in the northernmost region to the Northern Basin and Victoria Basin to beneath the Ross Ice Shelf. Notably, the zone of extremely low T_e values in the western Ross Sea widens to 350 km near Ross Island (Fig. 1), which is dominated by the southernmost active volcano (Mt. Erebus) in Antarctica, as well as extinct volcanoes (Mt. Bird and Mt. Terror) (Kyle, 1994). Based on seismic studies, a low-velocity anomaly exists in the upper mantle near Ross Island (Lawrence et al., 2006b; Watson et al., 2006). This anomaly may reflect crustal extension and the rise of magma (Jaupart and Mareschal, 2007) in the Cenozoic. Moreover, the deep ocean basin is also characterized by locally very low T_e values of approximately 5 km along the seaward continental

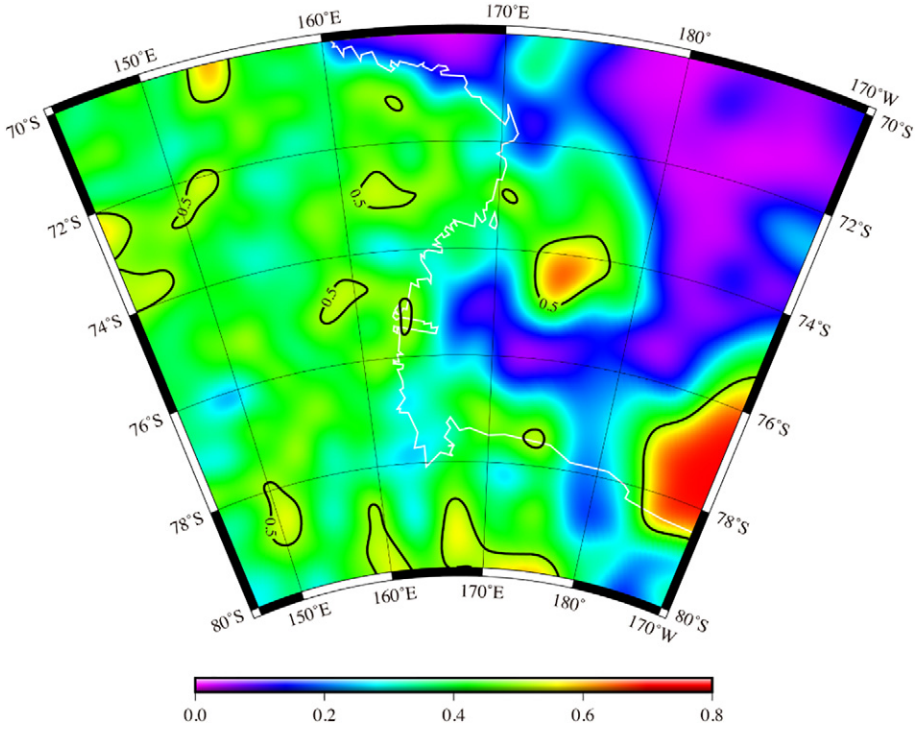

Fig. 4. The maximum values of the normalized squared imaginary component of the coherency between the free-air gravity anomaly and the topography (free-air NSIC) around the Bouguer transition wavelength. The contours illustrate the regions where free-air NSIC is larger than 0.5.

shelf. The two low-value zones are connected in the Adare Basin. In this paper, the discussion focuses on the basins on the continental shelf. The estimated T_e values in the other basins in Ross Sea reach 40 km, with an average of 35 km, and change little at the lateral margins of the structures, including the Coulman High, Central Trough, Central High, Eastern Basin and Ross Ice Shelf. The T_e values divide the extensional basins in the Ross Sea into two areas, the western Ross Sea features low flexural rigidity, and the other areas of the Ross Sea features higher flexural rigidity.

The T_e values of the continental lithosphere are relatively high and vary more widely. The Airy isostatic anomaly (Jordan et al., 2013) suggests that a major fault (blue line in Fig. 5) may exist as a boundary of

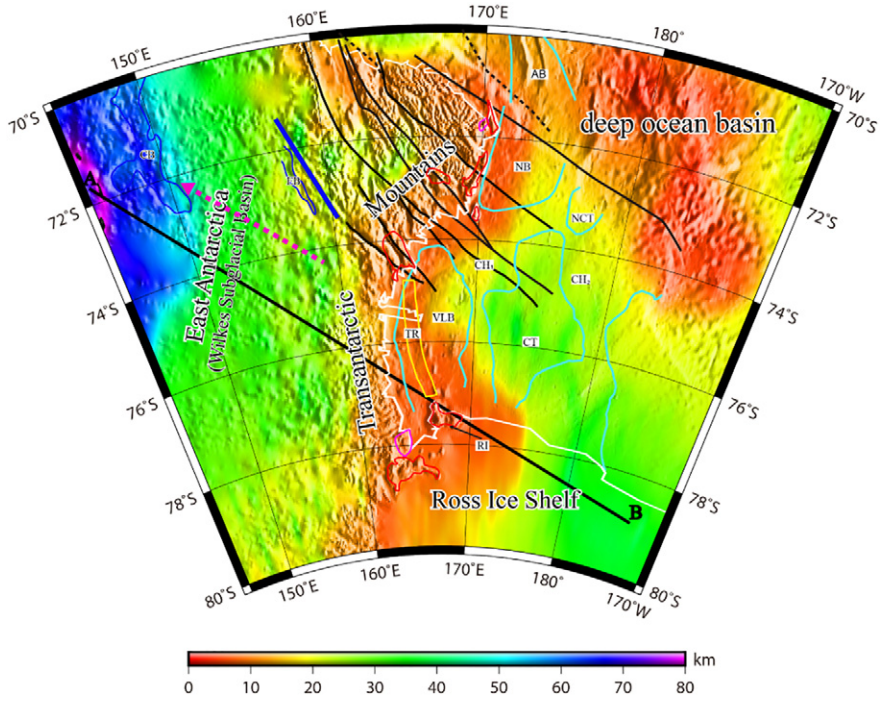

Fig. 5. Variations in the T_e values of the TAM and Ross Sea. To better orient the reader, subglacial topography has been superimposed on the colors as shading. The white line represents the coastline. The blue line shows the location of the inferred major faults and the pink arrow marks the direction in which the crust becomes thinner (Jordan et al., 2013). EB and CB refer to the eastern and central basins of the WSB. For other abbreviations and symbols, please refer to Fig. 1. The bold black line is the section line shown in Fig. 6. Tectonic lines and abbreviations are the same as in Fig. 1.

WSB and northern Victoria Land (NVL). Our T_e results show that there is a significant difference in lithospheric strength between WSB and NVL. However, this difference is not only limited in the two sides of the inferred fault; instead, it extends along the TAM, and it reflects the regional differences in the mechanical properties and deformation of the lithosphere. Generally, the variation in T_e is relatively simple and increases from the eastern flank of the TAM (~7 km) landward, peaking at approximately 80 km in the northwestern region far from the coastline which is associated with the interior of the Gondwanan continent (Jordan et al., 2013). The strong flexural rigidity in East Antarctica is consistent with the high T_e values found for continental cratons or Precambrian shields in other flexural studies (Pérez-Gussinyé et al., 2009; Zuber et al., 1989). Numerical models (van Wijk et al., 2008) indicate that the total lithospheric strength of the East Antarctic craton gradually decreases seaward and that the lithosphere in East Antarctica is stronger than that in the Ross Sea, which agrees with our estimated variations in T_e.

4.2. Comparison with previous results

Based on a 2D thin elastic plate equation, Stern and ten Brink (1989) and ten Brink et al. (1997) estimated the variations in T_e values in East Antarctica and the Ross Sea. In their flexural models, an elastic plate with a rifted edge at the TAMF (rather than a continuous one) is employed, and the loads include the ice sheet, thermal buoyancy, erosion and isostatic end load. The resulting model (Stern and ten Brink, 1989) shows the T_e increasing sharply from a value of 5 km at the TAMF to 115 km and that a constant value of 19 km is present in the Ross Sea. By using more detailed subglacial topography and gravity data, similar studies have shown that the T_e values rise to 85 km (ten Brink et al., 1997) and 70 km (Lawrence et al., 2006a) in East Antarctica. Our results are basically in agreement with the T_e values recovered from the continental region but provide more detailed information of T_e variations and new insights into the lithospheric deformation in this region (Fig. 6).

In the ocean region, Karner et al. (2005) set the T_e value to 30 km in a process-oriented gravity model in an attempt to determine the cause of the positive gravity anomalies in the extensional basins in the Ross Sea. Our results show that the T_e values are generally 35 km throughout the Ross Sea except for the TAMF, where the flexural rigidities are extremely low. Numerous studies have documented the crustal structure in the TAM and the surrounding regions via earthquakes recorded by deployed seismic stations and have observed significantly low seismic wave velocities and a thermal anomaly beneath Ross Island and the Terror Rift (Bannister et al., 2000; Lawrence et al., 2006b; Pyle et al., 2010; Watson et al., 2006). Moreover, high heat flow values have been measured along the TAMF (Morin et al., 2010). The evidence of the relationship between the mechanical strength of the lithosphere and the seismic wave velocity and heat flow has been demonstrated in several studies (Chen et al., 2015a; Lowry and Smith, 1995; Pérez-Gussinyé et al., 2007). The high heat flow and low seismic velocity are consistent with the low flexural rigidity observed in the western Ross Sea. Accordingly, the T_e map based on the Bouguer coherence presented in this paper can be used to explore the mechanical strength of the lithosphere with respect to previous results.

5. Discussion

5.1. T_e versus surface heat flow

Heat flow is proportional to the temperature gradient and is related to the thermal state of the lithosphere, and the internal heat processes in the Earth control many lithospheric properties and geological processes (Furlong and Chapman, 2013; Lowry and Smith, 1995). In general, the heat flow is high in tectonically active regions and low in stable cratons. As stated before, a correlation exists between heat flow and T_e, although the heat flow can be affected by numerous factors, such as crustal heat production and the dynamical effects of subduction, erosion, and hydrologic flow (Mareschal and Jaupart, 2004).

An et al. (2015) constructed a 3D S-wave model for the Antarctic plate and converted it into a 3D temperature model of the lithosphere. By constraining the temperature of bedrock and upper mantle, the distribution of surface heat flow for the Antarctic lithosphere was obtained using 1D steady state heat conduction (Fig. 7). However, the converted heat flow is only reliable when the surface heat flow is <90 mW/m^2 because tectonic processes can affect the validity of the results (An et al., 2015). The measured heat flow values were superimposed to on these results to test the validity of the model. The model yielded low heat flow values in the East Antarctica, which features an old, cold and thick continental craton. In contrast, at the TAMF, the heat flow model produced high values that largely coincide with measured values, revealing a high-temperature region that coincides with the low T_e zone. In this area, the measured heat flow is >70 mW/m^2. The relatively high thermal state may be related to mantle upwelling during the early extensional phase (Salvini et al., 1997). Additionally, the measured high heat flow values in the western Ross Sea correlates well with the studies of low seismic waves velocities, which show that the western Ross Sea has a hotter mantle (Lawrence et al., 2006b). However, the low values predicted by the model for the eastern Ross Sea disagree with the measured values. The less reliable heat flow values are primarily concentrated in the oceanic region where the model resolution is poor (An et al., 2015). Consequently, we hypothesize that the low heat

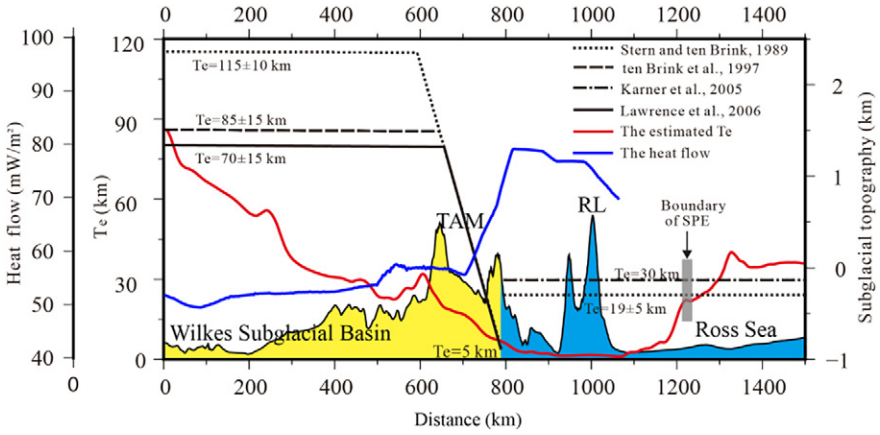

Fig. 6. The heat flow (after removal of invalid values) from An et al. (2015), estimated T_e values and bedrock topography across East Antarctica, the TAM and the Ross Sea. Previously estimated T_e results are also shown. The gray bar displays the possible location of eastern boundary of the Cenozoic extension zone that extends between approximately 800 and 1200 km if we consider that the TAMF is the western boundary. SPE, second phase of extension in the Cenozoic.

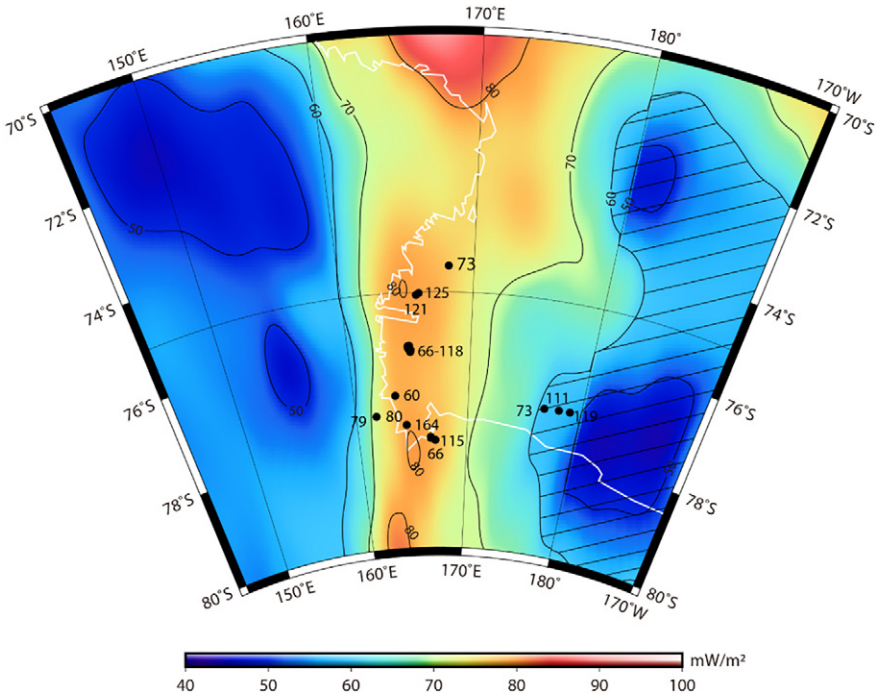

Fig. 7. Distribution of heat flow in the TAM and Ross Sea from An et al. (2015). The black dots indicate the measured heat flow values from The Global Heat Flow Database (http://www.heatflow.und.edu/index2.html). The shaded areas indicate the hypothesized invalid heat flow from An et al. (2015).

flow values in the eastern Ross Sea are invalid and remove them (shaded area in Fig. 6) in the next analysis. As for the remaining values, we cannot guarantee the validity of their absolute values, but they are consistent with the measured heat flow values (e.g., in the TAMF) and thermal regimes and reflect the current thermal state of the lithosphere in the Eastern Antarctica and the TAMF. The comparison of the heat flow data with T_e in Fig. 6 reveals a distinct negative correlation between heat flow and T_e in the East Antarctica and the western Ross Sea, which suggests that the relationship between thermal state and the mechanical strength of the lithosphere is relatively simple. This negative correlation may be associated with the Cenozoic crustal extension in western Ross Sea that has reduced the strength of the lithosphere.

In general, as shown in Fig. 7, the heat flow values in East Antarctica are very low, suggesting that it is a typical stable craton, whereas the heat flow values in the TAMF and the western Ross Sea are high. These high values extend from Ross Island in the south to the northernmost Adare Basin, where seafloor spreading occurred from 43 to 26 Ma (Cande and Kent, 1995). Combined with the subsequent normal faulting and uplift of the Adare Trough, we suggest that several phases of spreading and post-spreading tectonic activity in the Adare Basin (Granot et al., 2010) are responsible for the present thermal state of the crust. For the East Basin, even though the heat flow values from An et al. (2015) are invalid, we speculate that they are likely to be relatively high based on the few measured heat flow data that are available from the eastern Ross Sea and the Mesozoic rifting history of this area (Behrendt et al., 1991).

5.2. Ross Sea

For oceanic crust, T_e primarily represents the strength of the lithosphere at the time of loading and is thus a function of the temperature gradient of the lithosphere (Watts, 2001, 1978). Therefore, if loading occurs at a certain T_e and no subsequent mass redistribution occurs, such as erosion or deposition, our results yield the same flexural rigidity even after cooling and strengthening of the lithosphere. Consequently, it is critical to determine the type of crust (continental or oceanic) beneath the extensional basins in the Ross Sea. Davey et al. (2006) interpreted the structure of the Northern Basin to be oceanic crust or transitional crust. Cande and Stock (2006) suggested that the crust of the Northern Basin may be transitional based on the magnetic anomaly data. The OBS profile and gravity model produced by the ACRUP project implies that the densities of crustal rocks increase from the Coulman High to the Eastern Basin and vary between 2.65 g/cm^3 and 2.95 g/cm^3 (Trey et al., 1999). Therefore, we consider the thinned crust in the Ross Sea to be oceanic crust.

The relatively high T_e values in the Ross Sea indicate that the flexural rigidity is high in basins filled with sediment and that no subsequent tectonic activity has altered the thermal state of the underlying lithosphere. The results of drilling in the south-central Ross Sea and Cape Robert area show that the oldest sediments were not deposited earlier than the Eocene and that approximately three-quarters of the sediments are Neogene in age (Barrett, 1989, 1975). Because the Mesozoic extensional event ended at 85 Ma (Fitzgerald et al., 1986), the basins in the Ross Sea were starved of sediment for over 40 Ma until rapid deposition began following the Eocene. Due to this considerable time lag, we suggest that the lithosphere had become strong and cold by the time of sediment loading due to heat diffusion. This explanation is consistent with the ideas of Karner et al. (2005), who argued that the positive gravity anomalies in the three Ross Sea basins are due to the high flexural rigidity of the lithosphere that developed between the end of rifting and the beginning of sedimentation.

The thermal perturbations that occur beneath the hotspots, e.g., the Afar hotspot beneath Africa and volcanic provinces likely led to the direct rejuvenation of the thermal state of the lithosphere and the reduction of its mechanical strength (Pérez-Gussinyé et al., 2009; Ratheesh Kumar and Windley, 2013). The T_e of the entire extensional basins of the Ross Sea might have been as high as 35 km if the later episode of thermally related tectonic activity, namely Cenozoic extension in the western Ross Sea, had not occurred. However, the extensional activity during the Cenozoic in the western Ross Sea rejuvenated the lithosphere, resulting in the low T_e values seen in the TAMF. Based on the abrupt change (decrease) of T_e in the western Ross Sea (Fig. 6), the location of the $T_e = 15$ km contour essentially indicates the horizontal temperature gradient or a thermal boundary in the lithosphere between the

areas affected by Cenozoic and Mesozoic tectonic activities. In addition, the relatively high T_e values in the eastern Ross Sea indicate that the strength of the lithosphere has been maintained since it has not been affected by the additional thermal perturbations after the period of extension in Mesozoic. Considering the strong correlation between T_e and heat flow discovered in the study region (Fig. 6), we speculate that the lithosphere in the eastern Ross Sea is colder than that in the western Ross Sea, but warmer than that in East Antarctica. Consequently, based on the variations of thermal regime of the lithosphere, we divide the entire study region into a "cold zone" in East Antarctica, a "hot zone" in the western Ross Sea and "warm zone" in the eastern Ross Sea (Fig. 8). Previous tectonic events are intimately related to the regional thermal evolution, and rift areas are generally characterized by low T_e values. Although the relationship between tectonics, mechanical strength and thermal regime is not very specific, we assume a model (Fig. 8) that considers the thermal boundary to be the tectonic boundary between the two phases of extension in the Ross Sea. If so, the extensional activity in the Cenozoic occurred in the western Ross Sea and was approximately 200–400 km in width, including the Adare Basin, Northern Basin, Terror Rift and Ross Island. The Victoria Land Basin formed in the Cretaceous but may have been thermally affected by the later extension.

5.3. TAM and East Antarctica (WSB)

The variations in T_e in the continent from the TAM to WSB are relatively simple, and the gradually increasing trend coincides with the results estimated by Stern and ten Brink (1989), ten Brink et al. (1997) and Lawrence et al. (2006a), who proposed models that are based on the assumption that the TAMF is a rifted edge. The study of airborne gravity data (Jordan et al., 2013) suggested that some degree of local isostatic compensation in the WSB seems to better fit the observed gravity signatures, suggesting that a broken flexural plate model is not suitable here. Nevertheless, considering the limited constraints from geophysical data in the gravity model, the relatively strong flexural rigidity (T_e = 30–80 km) that we estimated for WSB seems to favor the flexural model. Recent study of seismic data from TAMNNET (Hansen et al., 2016) also supports the flexural model for WSB and TAM, as do previous studies (Stern and ten Brink, 1989; ten Brink and Stern, 1992; ten Brink et al., 1997).

Moreover, the distribution of T_e over continents (Audet and Bürgmann, 2011) suggests that continental margins, which are characterized by low values of T_e, are repeatedly weakened and deformed during rifting, whereas continental cores tend to remain intact and strong. Tesauro et al. (2012) have also argued that the opening of oceanic basins significantly thermally weakens the continental margins during rifting. The Afar triple junction provides a remarkable example of the weakened continental margins. Pérez-Gussinyé et al. (2009) and Chen et al. (2015b) used the improved multitaper method and fan wavelet analysis to acquire a map of T_e values in this area, and the results of both methods show that the flexural strength gradually increases from the rifted Red Sea and Gulf of Aden to the adjacent old Arabian Plate and Africa Plate. These changes are similar to the changes in T_e that we observed at the rifted margin of the East Antarctica craton. Our results in the East Antarctica favor the idea that the TAMF, as a wing of the extension of the WARS, represents the boundary between East and West Antarctica. Here, a schematic model of a rigid lithospheric plate overlying asthenosphere is employed to interpret the features of T_e values observed in the continent (Fig. 9). We suggest that normal faulting occurred along the continental margin and within the highly stretched lithosphere during extension (An et al., 2015), contributing to the gradual decrease in T_e values from East Antarctica to the TAM. During extension, the faults cut the upper crust and reduced the mechanical strength of the upper part of lithosphere. Massive normal faults are observed along the eastern margin of the TAM and in the western Ross Sea (Hall et al., 2007; Salvini et al., 1997). Thinning of the lithosphere and mantle upwelling due to the two phases of extension weakened the bottom of the lithosphere. Moreover, some decoupling between the lower and upper crust may have occurred (van Wijk et al., 2008), favoring reductions in T_e.

Apatite fission track analysis (Fitzgerald, 1994, 1992) indicates that the uplift of the TAM began around 55 Ma in the Cenozoic and the maximum uplift was approximately 6 km. This phase was accompanied by

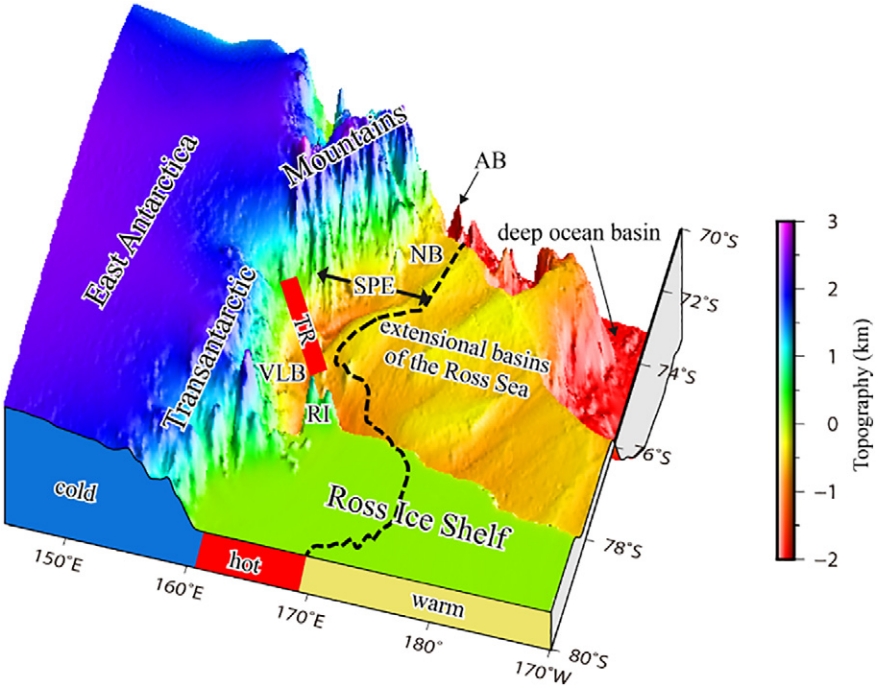

Fig. 8. The 3D topography of the Ross Sea region showing the possible tectonic boundaries between the areas affected by Cenozoic and Mesozoic extensional events (colors represent elevation). SPE, second phase of extension in the Cenozoic. For other notations, please refer to Fig. 1. The black dashed line is the spatial distribution of T_e = 15, shown as the gray bar in Fig. 6. The different colors along the front face represent the current thermal regimes in the lithosphere beneath the study region.

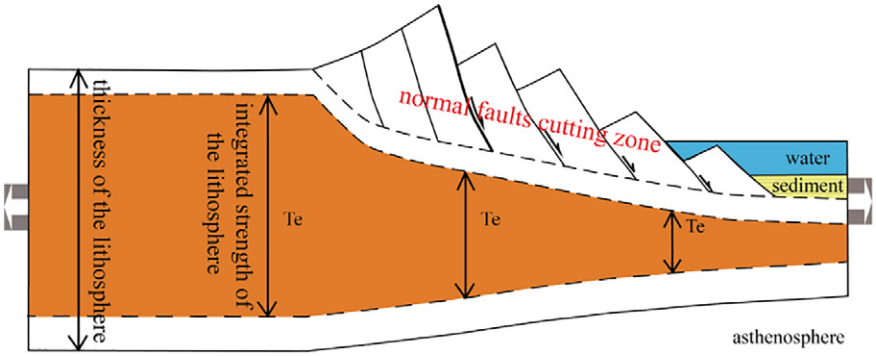

Fig. 9. Schematic model of a rifted continental margin illustrating the crustal thinning and normal faults due to tectonic extension, which weakens the mechanical strength of crust and reduces the T_e. The blank area indicates approximate location of normal faults that cut the crust. The T_e reflect integrated brittle, elastic and ductile strength of the entire lithosphere and it is less than the thickness of the lithosphere. Thus, we assumed an initial T_e before thinning of the lithosphere and normal faults occurred.

magmatism in the western Ross Sea. Stern and ten Brink (1989) suggested that lateral thermal conduction occurred between hot, thin, young lithosphere in the Ross Basin and the cold, thick, old East Antarctica craton, which provided a thermally buoyant load beneath the TAMF that aided in the uplift of the TAM. The numerical models also show that elevated temperatures contributed to the uplift of the TAM and that the convergence of crustal material has helped maintain the current height of the TAM (van Wijk et al., 2008). Seismic and gravity data from this area have been interpreted as reflecting a thermal contrast between East Antarctica and the western Ross Sea (Hansen et al., 2016; Lawrence et al., 2006a, b; Watson et al., 2006). A seismic velocity model shows the crust beneath the TAM is only approximately 5 km thicker (Lawrence et al., 2006a). This result indicates that the TAM is not locally compensated, which seems to contradict our results because the local (Airy) isostasy implied by our low T_e estimates requires a much deeper root. Consequently, we argue that the TAM is possibly supported by the detected buoyancy driven by the hotter mantle material beneath western Ross Sea, rather than the mechanical strength of the lithosphere. Until now, however, the degree to which this force contributes to the uplift of the TAM has remained unknown. Based on the free-edge elastic plate model, Stern et al. (2005) found that the isostatic rebound as a response to glacial incision in the TAM increased as much as 50% of the elevation (about 2000 m), resulting in the present-day observed topography. Bialas et al. (2007) proposed an alternative model and indicated that the TAM and the crustal root are the remnant of the collapse of a plateau prior to continental extension. This model showed that TAM had an elevation of 1–2 km at the end of the Cretaceous. Van Wijk et al. (2008) suggested that a tectonic force existed in the TAMF. This force resulted in the convergence of crustal material and the uplift of the surface topography. However, to determine whether thermal buoyancy contributes to the elevation of the TAM and the degree of its contribution, it will be necessary to use numerical modeling or geodynamic approaches. At the present, a single uplift mechanism fails to explain the present elevation of the TAM, and a hybrid model seems to be needed.

The widespread regional NW-SE dextral strike-slip faults located in the NVL and the adjacent Ross Sea reach lengths of over 800 km and may have been driven by transform faults related to the movement of plates in the Cenozoic and likely the Late Eocene (Salvini et al., 1997). Burov and Diament (1995) suggested that lithospheric flexural strength decreases significantly when intracontinental faults form. However, it seems that the appearance of these faults failed to affect or change the variation trends of T_e in the NVL, which exhibit similar decrease trends of T_e compared with the southern Victoria Land. This poor correlation between T_e and the distribution of large-scale strike-slip faults is likely because the faults occur in the region where the lithosphere has been weakened by rifting. We argue that the lithospheric rifting has been the primary driver of the reduction of the strength of the lithosphere. In other words, we suggest that the effects of thinning of the lithosphere or the crust on the T_e values at the continental margin are likely to be much stronger than those of the rifting-related faults or the subsequent faults. Consequently, the flexural rigidity of several passive continental margins around the world should exhibit similar features.

6. Conclusions

In this study, we have generated T_e map over the TAM and the Ross Sea by estimating the coherence of the Bouguer gravity anomaly and the topography based on fan wavelet analysis. The highest T_e values (~80 km) are located in the old and cold East Antarctic continent, whereas the lowest values are located at the TAMF due to the Cenozoic extension in the western Ross Sea. The T_e values in the other extensional basins of the Ross Sea besides the TAMF are on the order of 35 km, indicative of the flexural rigidity when the sediments filled the basins. Our results correlate well with previous T_e estimates for the continental and oceanic regions. We also find that the variations in T_e are generally consistent with surface heat flow data and lithospheric tectonic units. This analysis of T_e has allowed us to reach the following conclusions.

1. Our T_e map delineates the rifting boundary between the eastern and western portions of the Antarctic continent. The gradual reduction in flexural rigidity from East Antarctica to the TAMF is a result of a combination of normal faults in the TAMF and thinning of the lithosphere. However, the effects of Cenozoic NW-SE-oriented right-lateral strike-slip faults in NVL on the lithospheric flexural rigidity remain unclear. The effects of these faults were likely attenuated by the early extension in the late Cretaceous.
2. The Cenozoic extension in the western Ross Sea thermally rejuvenated the underlying lithosphere and reduced its mechanical strength, as reflected by the low T_e values zone in our results for the TAMF. Based on the relationship between tectonics and mechanical strength of lithosphere, we have identified the tectonic boundary between the Cenozoic and Mesozoic extensional events. The Northern Basin, Terror Rift and Ross Island are associated with the Cenozoic event.
3. The relatively high T_e values observed in the Ross Sea extensional basins are the result of the time lag in filling of the basins at the end of late Cretaceous extension. The mechanical strength increased due to the long duration of thermal dissipation (over 40 Ma).
4. The large deformation (low T_e) and shallow crustal root beneath the TAM suggests that a buoyant thermal load (ten Brink et al., 1997) in upper mantle partially supports the TAM rather than local (Airy) isostasy.

Acknowledgements

This research was supported by the National Science Foundation of China (No. 41576069), the China Postdoctoral Science Foundation (No. 2016M601925) and the Chinese Polar Environment Comprehensive

Investigation and Assessment Programmes (CHINARE 2017-01-03 and 2017-04-01). We are grateful to Dr. Jonathan F Kirby for providing the wavelet coherence analysis codes that we used in calculating the lithospheric elastic thickness variations. We thank Qingsheng Guan for his help with drawing Fig. 8. We are grateful for the constructive comments and suggestions from two anonymous reviewers. All of the projected figures in this paper are drawn using the GMT package developed by Wessel and Smith (1998).

References

Agostinetti, P., Roselli, P., Cattaneo, M., Amato, A., 2005. Moho-depth and subglacial sedimentary layer thickness in the Wilkes Basin from receiver function analysis. IASPEI. General Assembly, October 2.9, 2005, Chile, Abstracts Volume, pp. 281–284.

Amante, C., Eakins, B.W., 2009. ETOPO1 1 arc-minute global relief model: procedures, data sources and analysis. NOAA Technical Memorandum NESDIS NGDC-24.

An, M., Wiens, D.A., Zhao, Y., Feng, M., Nyblade, A., Kanao, M., Li, Y., Maggi, A., Lévêque, J.-J., 2015. Temperature, lithosphere-asthenosphere boundary, and heat flux beneath the Antarctic Plate inferred from seismic velocities. J. Geophys. Res. Solid Earth 120: 8720–8742. http://dx.doi.org/10.1002/2015JB011917.

Audet, P., Bürgmann, R., 2011. Dominant role of tectonic inheritance in supercontinent cycles. Nat. Geosci. 4:184–187. http://dx.doi.org/10.1038/ngeo1080.

Bannister, S., Snieder, R.K., Passier, M.L., 2000. Shear-wave velocities under the Transantarctic Mountains and terror rift from surface wave inversion. Geophys. Res. Lett. 27:281–284. http://dx.doi.org/10.1029/1999GL010866.

Barrett, P.J., 1975. Textural Characteristics of Cenozoic Preglacial and Glacial Sediments at Site 270, Ross Sea, Antarctica, Initial Reports of the Deep Sea Drilling Project. International Ocean Discovery Program (IODP), Washington, D.C.

Barrett, P.J., 1989. Antarctic Cenozoic History From CIROS-1 Drill Hole, McMurdo Sound, DSIR Bulletin 245. Science Information Publishing Center, Wellington.

Behrendt, J.C., LeMasurier, W.E., Cooper, A.K., Tessensohn, F., Tréhu, A., Damaske, D., 1991. Geophysical studies of the west Antarctic rift system. Tectonics 10:1257–1273. http://dx.doi.org/10.1029/91TC00868.

Bialas, R.W., Buck, W.R., Studinger, M., Fitzgerald, P.G., 2007. Plateau collapse model for the Transantarctic Mountains–west Antarctic Rift system: insights from numerical experiments. Geology 35:687–690. http://dx.doi.org/10.1130/G23825A.1.

Blackman, D.K., von Herzen, R.P., Lawver, L.A., 1987. Heat flow and tectonics in the western Ross Sea, Antarctica. In: Cooper, A.K., Davey, F.J. (Eds.), The Antarctic Continental Margin: Geology and Geophysics of the Western Ross Sea. Vol. 5B. Circum-Pacific Council for Energy and Mineral Resources, Houston, TX, pp. 179–189.

Bodine, J.H., Steckler, M.S., Watts, A.B., 1981. Observations of flexure and the rheology of the oceanic lithosphere. J. Geophys. Res. 86:3695. http://dx.doi.org/10.1029/JB086iB05p03695.

Braitenberg, C., Wang, Y., Fang, J., Hsu, H.T., 2003. Spatial variations of flexure parameters over the Tibet–Quinghai plateau. Earth Planet. Sci. Lett. 205:211–224. http://dx.doi.org/10.1016/S0012-821X(02)01042-7.

Burov, E.B., Diament, M., 1995. The effective elastic thickness (Te) of continental lithosphere: what does it really mean? J. Geophys. Res. 100:3905–3927. http://dx.doi.org/10.1029/94JB02770.

Cande, S.C., Kent, D.V., 1995. Revised calibration of the geomagnetic polarity timescale for the Late Cretaceous and Cenozoic. J. Geophys. Res. 100:6093–6095. http://dx.doi.org/10.1029/94JB03098.

Cande, S.C., Stock, J.M., 2006. Constraints on the timing of extension in the Northern Basin, Ross Sea. International Symposium on Antarctic Earth Science. Springer, Antarctica, pp. 319–326.

Cande, S.C., Stock, J.M., Müller, R.D., Ishihara, T., 2000. Cenozoic motion between east and west Antarctica. Nature 404:145–150. http://dx.doi.org/10.1038/35004501.

Chen, B., Chen, C., Kaban, M.K., Du, J., Liang, Q., Thomas, M., 2013. Variations of the effective elastic thickness over China and surroundings and their relation to the lithosphere dynamics. Earth Planet. Sci. Lett. 363:61–72. http://dx.doi.org/10.1016/j.epsl.2012.12.022.

Chen, B., Kaban, M.K., El Khrepy, S., Al-Arifi, N., 2015a. Effective elastic thickness of the Arabian plate: weak shield versus strong platform. Geophys. Res. Lett. 42: 3298–3304. http://dx.doi.org/10.1002/2015GL063725.

Chen, B., Liu, J., Chen, C., Du, J., Sun, Y., 2015b. Elastic thickness of the Himalayan–Tibetan orogen estimated from the fan wavelet coherence method, and its implications for lithospheric structure. Earth Planet. Sci. Lett. 409:1–14. http://dx.doi.org/10.1016/j.epsl.2014.10.039.

Cooper, A.K., Davey, F.J., Behrendt, J.C., 1987. Seismic stratigraphy and structure of the Victoria Land basin, western Ross Sea, Antarctica. In: Cooper, A.K., Davey, F.J. (Eds.), The Antarctic Continental Margin: Geology and Geophysics of the Western Ross Sea. Vol. 5B. Circum-Pacific Council for Energy and Mineral Resources, Houston, TX, pp. 27–76.

Damaske, D., Läufer, A.L., Goldmann, F., Möller, H.D., Lisker, F., 2007. Magnetic anomalies northeast of Cape Adare, northern Victoria Land (Antarctica), and their relation to onshore structure. In: Cooper, A.K., et al. (Eds.), Proceedings of the 10th ISAES X Antarctica: A Keystone in a Changing World-Online, U.S. Geological Survey. Open-file Rep., 2007–1047, Short Research Paper 016, p. 5.

Davey, F.J., Cande, S.C., Stock, J.M., 2006. Extension in the western Ross Sea region-links between Adare Basin and Victoria Land Basin. Geophys. Res. Lett. 33, L20315. http://dx.doi.org/10.1029/2006GL027383.

Dorman, L.M., Lewis, B.T.R., 1970. Experimental isostasy: 1. Theory of the determi- nation of the earth's isostatic response to a concentrated load. J. Geophys. Res. 75: 3357–3365. http://dx.doi.org/10.1029/JB075i017p03357.

Drewry, D.J., 1976. Sedimentary basins of the east antarctic craton from geophysical evidence. Tectonophysics 36:301–314. http://dx.doi.org/10.1016/0040-1951(76)90023-8.

Ferraccioli, F., Armadillo, E., Jordan, T.A., Bozzo, E., Corr, H., 2009. Aeromagnetic exploration over the East Antarctic ice sheet: a new view of the Wilkes Subglacial Basin. Tectonophysics 478:62–77. http://dx.doi.org/10.1016/j.tecto.2009.03.013.

Fitzgerald, P.G., 1992. The Transantarctic Mountains of southern Victoria land: the application of apatite fission track analysis to a rift shoulder uplift. Tectonics 11:634–662. http://dx.doi.org/10.1029/91TC02495.

Fitzgerald, P.G., 1994. Thermochronologic constraints on post-Paleozoic tectonic evolution of the central Transantarctic Mountains, Antarctica. Tectonics 13:818–836. http://dx.doi.org/10.1029/94TC00595.

Fitzgerald, P.G., Sandiford, M., Barrett, P.J., Gleadow, A.J.W., 1986. Asymmetric extension associated with uplift and subsidence in the Transantarctic Mountains and Ross Embayment. Earth Planet. Sci. Lett. 81:67–78. http://dx.doi.org/10.1016/0012-821X(86)90101-9.

Fitzsimons, I.C.W., 2003. Proterozoic basement provinces of southern and southwestern Australia, and their correlation with Antarctica. Geol. Soc. Lond., Spec. Publ. 206: 93–130. http://dx.doi.org/10.1144/GSL.SP.2003.206.01.07.

Förste, C., Bruinsma, S.L., Shako, R., Abrikosov, O., Flechtner, F., Marty, J.-C., Lemoine, J.-M., Dahle, C., Neumeyer, H., Barthelmes, F., Biancale, R., Balmino, G., König, R., 2012. A new release of EIGEN-6: the latest combined global gravity field model including LAGEOS, GRACE and GOCE data from the collaboration of GFZ Potsdam and GRGS Toulouse. Geophys. Res. Abstr. 14, 2821–2822 (EGU General Assembly).

Forsyth, D.W., 1985. Subsurface loading and estimates of the flexural rigidity of continental lithosphere. J. Geophys. Res. 90:12623. http://dx.doi.org/10.1029/JB090iB14p12623.

Fretwell, P., Pritchard, H.D., Vaughan, D.G., Bamber, J.L., Barrand, N.E., Bell, R., Bianchi, C., Bingham, R.G., Blankenship, D.D., Casassa, G., Catania, G., Callens, D., Conway, H., Cook, A.J., Corr, H.F.J., Damaske, D., Damm, V., Ferraccioli, F., Forsberg, R., Fujita, S., Gim, Y., Gogineni, P., Griggs, J.A., Hindmarsh, R.C.A., Holmlund, P., Holt, J.W., Jacobel, R.W., Jenkins, A., Jokat, W., Jordan, T., King, E.C., Kohler, J., Krabill, W., Riger-Kusk, M., Langley, K.A., Leitchenkov, G., Leuschen, C., Luyendyk, B.P., Matsuoka, K., Mouginot, J., 2013. Bedmap2: improved ice bed, surface and thickness datasets for Antarctica. Cryosphere 7:375–393. http://dx.doi.org/10.5194/tc-7-375-2013.

Furlong, K.P., Chapman, D.S., 2013. Heat flow, heat generation, and the thermal state of the lithosphere. Annu. Rev. Earth Planet. Sci. 41:385–410. http://dx.doi.org/10.1146/annurev.earth.031208.100051.

Gao, J.Y., Yang, C.G., Zhang, T., Wu, Z.C., Shen, Z.Y., Wang, W., 2015. Calculation of terrain and isostatic gravity effects in Antarctica and its surroundings. Hydrogr. Surveying Charting. 35, pp. 1671–3044.

Granot, R., Cande, S.C., Stock, J.M., Davey, F.J., Clayton, R.W., 2010. Postspreading rifting in the Adare Basin, Antarctica: regional tectonic consequences. Geochem. Geophys. Geosyst. 11, Q08005. http://dx.doi.org/10.1029/2010GC003105.

Grikurov, G.E., 1982. Structure of Antarctica and outline of its evolution. In: Craddock, C. (Ed.), Antarctic Geoscience—Symposium on Antarctic Geology and Geophysics. University of Wisconsin Press, Madison, Wisconsin, pp. 791–804.

Hall, J.M., Wilson, T.J., Henrys, S., 2007. Structure of the central Terror Rift, western Ross Sea, Antarctica. In: Cooper, A.K., Raymond, C.R., The 10th ISAES Editorial Team (Eds.), Antarctica: A Keystone in a Changing World – Online Proceedings of the 10th ISAES, USGS Open-file Report 2007–1047, Short Research Paper 108 http://dx.doi.org/10.3133/of2007-1047.srp108.

Hansen, S.E., Kenyon, L.M., Graw, J.H., Park, Y., Nyblade, A.A., 2016. Crustal structure beneath the Northern Transantarctic Mountains and Wilkes Subglacial Basin: implications for tectonic origins. J. Geophys. Res. Solid Earth 121:812–825. http://dx.doi.org/10.1002/2015JB012325.

Jaupart, C., Mareschal, J.C., 2007. Heat flow and thermal structure of the lithosphere. In: Watts, A.B. (Ed.), Treatise on Geophysics. Elsevier BV, London, pp. 217–251.

Jordan, T.A., Ferraccioli, F., Armadillo, E., Bozzo, E., 2013. Crustal architecture of the Wilkes Subglacial Basin in East Antarctica, as revealed from airborne gravity data. Tectonophysics 585:196–206. http://dx.doi.org/10.1016/j.tecto.2012.06.041.

Karner, G.D., Studinger, M., Bell, R.E., 2005. Gravity anomalies of sedimentary basins and their mechanical implications: application to the Ross Sea basins, west Antarctica. Earth Planet. Sci. Lett. 235:577–596. http://dx.doi.org/10.1016/j.epsl.2005.04.016.

Kirby, J.F., 2005. Which wavelet best reproduces the Fourier power spectrum? Comput. Geosci. 31:846–864. http://dx.doi.org/10.1016/j.cageo.2005.01.014.

Kirby, J.F., Swain, C.J., 2004. Global and local isostatic coherence from the wavelet transform. Geophys. Res. Lett. 31:124608. http://dx.doi.org/10.1029/2004GL021569.

Kirby, J.F., Swain, C.J., 2008. An accuracy assessment of the fan wavelet coherence method for elastic thickness estimation. Geochem. Geophys. Geosyst. 9, Q03022. http://dx.doi.org/10.1029/2007GC001773.

Kirby, J.F., Swain, C.J., 2009. A reassessment of spectral te estimation in continental interiors: the case of North America. J. Geophys. Res. 114, B08401. http://dx.doi.org/10.1029/2009JB006356.

Kirby, J.F., Swain, C.J., 2011. Improving the spatial resolution of effective elastic thickness estimation with the fan wavelet transform. Comput. Geosci. 37:1345–1354. http://dx.doi.org/10.1016/j.cageo.2010.10.008.

Kirby, J.F., Swain, C.J., 2014. The long-wavelength admittance and effective elastic thickness of the Canadian Shield. J. Geophys. Res. Solid Earth 119:5187–5214. http://dx.doi.org/10.1002/2013JB010578.

Kyle, P.R., 1994. Volcanological and Environmental Studies of Mount Erebus, Antarctica. American Geophysical Union, Washington DC.

Laske, G., Masters, G., Ma, Z., Pasyanos, M., 2013. Update on CRUST1.0 – A 1-degree global model of Earth's crust. Geophys. Res. Abstr. 15 (Abstract EGU2013–2658).

Lawrence, J.F., Wiens, D.A., Nyblade, A.A., Anandakrishnan, S., Shore, P.J., Voigt, D., 2006a. Crust and upper mantle structure of the Transantarctic Mountains and surrounding

regions from receiver functions, surface waves, and gravity: implications for uplift models. Geochem. Geophys. Geosyst. 7, Q10011. http://dx.doi.org/10.1029/2006GC001282.
Lawrence, J.F., Wiens, D.A., Nyblade, A.A., Anandakrishan, S., Shore, P.J., Voigt, D., 2006b. Upper mantle thermal variations beneath the Transantarctic Mountains inferred from teleseismic S-wave attenuation. Geophys. Res. Lett. 33, L03303. http://dx.doi.org/10.1029/2005GL024516.
Lowry, A.R., Smith, R.B., 1995. Strength and rheology of the western U.S. Cordillera. J. Geophys. Res. 100:17947–17963. http://dx.doi.org/10.1029/95JB00747.
Mao, X., Wang, Q., Liu, S., Xu, M., Wang, L., 2012. Effective elastic thickness and mechanical anisotropy of South China and surrounding regions. Tectonophysics 550–553:47–56. http://dx.doi.org/10.1016/j.tecto.2012.05.019.
Mareschal, J.C., Jaupart, C., 2004. Variations of surface heat flow and lithospheric thermal structure beneath the North American craton. Earth Planet. Sci. Lett. 223:65–77. http://dx.doi.org/10.1016/j.epsl.2004.04.002.
McKenzie, D., 1978. Some remarks on the development of sedimentary basins. Earth Planet. Sci. Lett. 40:25–32. http://dx.doi.org/10.1016/0012-821X(78)90071-7.
McKenzie, D., 2003. EstimatingTein the presence of internal loads. J. Geophys. Res. 108: 2438. http://dx.doi.org/10.1029/2002JB001766.
Morin, R.H., Williams, T., Henrys, S.A., Magens, D., Niessen, F., Hansaraj, D., 2010. Heat flow and hydrologic characteristics at the AND-1B borehole, ANDRILL McMurdo Ice Shelf project, Antarctica. Geosphere 6:370–378. http://dx.doi.org/10.1130/GES00512.1.
Pérez-Gussinyé, M., Lowry, A.R., Watts, A.B., Velicogna, I., 2004. On the recovery of effective elastic thickness using spectral methods: examples from synthetic data and from the Fennoscandian shield. J. Geophys. Res. 109, B10409. http://dx.doi.org/10.1029/2003JB002788.
Pérez-Gussinyé, M., Lowry, A.R., Watts, A.B., 2007. Effective elastic thickness of South America and its implications for intracontinental deformation. Geochem. Geophys. Geosyst. 8, Q05009. http://dx.doi.org/10.1029/2006GC001511.
Pérez-Gussinyé, M., Metois, M., Fernández, M., Vergés, J., Fullea, J., Lowry, A.R., 2009. Effective elastic thickness of Africa and its relationship to other proxies for lithospheric structure and surface tectonics. Earth Planet. Sci. Lett. 287:152–167. http://dx.doi.org/10.1016/j.epsl.2009.08.004.
Pyle, M.L., Wiens, D.A., Nyblade, A.A., Anandakrishnan, S., 2010. Crustal structure of the Transantarctic Mountains near the Ross Sea from ambient seismic noise tomography. J. Geophys. Res. 115, B11310. http://dx.doi.org/10.1029/2009JB007081.
Ratheesh Kumar, R.T., Windley, B.F., 2013. Spatial variations of effective elastic thickness over the Ninetyeast Ridge and implications for its structure and tectonic evolution. Tectonophysics 608:847–856. http://dx.doi.org/10.1016/j.tecto.2013.07.034.
Robinson, E.S., Splettstoesser, J.F., 1984. Structure of the Transantarctic Mountains determined from geophysical surveys. In: Turner, M.D., Splettstoesser, J.F. (Eds.), Geology of the Central Transantarctic Mountains. Vol. 36. AGU, Washington, D.C., pp. 119–162.
Salvini, F., Brancolini, G., Busetti, M., Storti, F., Mazzarini, F., Coren, F., 1997. Cenozoic geodynamics of the Ross Sea region, Antarctica: crustal extension, intraplate strike-slip faulting, and tectonic inheritance. J. Geophys. Res. 102:24669–24696. http://dx.doi.org/10.1029/97JB01643.
Smith, A.G., Drewry, D.J., 1984. Delayed phase change due to hot asthenosphere causes Transantarctic uplift? Nature 309:536–538. http://dx.doi.org/10.1038/309536a0.
Stern, T.A., ten Brink, U.S., 1989. Flexural uplift of the Transantarctic Mountains. J. Geophys. Res. 94:10315–10330. http://dx.doi.org/10.1029/JB094iB08p10315.
Stern, T.A., Baxter, A.K., Barrett, P.J., 2005. Isostatic rebound due to glacial erosion within the Transantarctic Mountains. Geology 33:221. http://dx.doi.org/10.1130/G21068.1.
Storti, F., Rossetti, F., Salvini, F., 2001. Structural architecture and displacement accommodation mechanisms at the termination of the Priestley Fault, northern Victoria land, Antarctica. Tectonophysics 341:141–161. http://dx.doi.org/10.1016/S0040-1951(01)00198-6.
Studinger, M., Bell, R.E., Buck, W.R., Karner, G.D., Blankenship, D.D., 2004. Sub-ice geology inland of the Transantarctic Mountains in light of new areogeophysical data. Earth Planet. Sci. Lett. 220:391–408. http://dx.doi.org/10.1016/S0012-821X(04)00066-4.
Sugden, D., Denton, G., 2004. Cenozoic landscape evolution of the convoy range to Mackay glacier area, Transantarctic Mountains: onshore to offshore synthesis. Geol. Soc. Am. Bull. 116:840. http://dx.doi.org/10.1130/B25356.1.
Swain, C.J., Kirby, J.F., 2003. The effect of 'noise' on estimates of the elastic thickness of the continental lithosphere by the coherence method. Geophys. Res. Lett. 30. http://dx.doi.org/10.1029/2003GL017070.
Tassara, A., Swain, C., Hackney, R., Kirby, J., 2007. Elastic thickness structure of South America estimated using wavelets and satellite-derived gravity data. Earth Planet. Sci. Lett. 253:17–36. http://dx.doi.org/10.1016/j.epsl.2006.10.008.
ten Brink, U., Stern, T., 1992. Rift flank uplifts and Hinterland Basins: comparison of the Transantarctic Mountains with the great escarpment of southern Africa. J. Geophys. Res. 97:569. http://dx.doi.org/10.1029/91JB02231.
ten Brink, U.S., Bannister, S., Beaudoin, B.C., Stern, T.A., 1993. Geophysical inverstigations of the tectonic boundary between East and West Antarctica. Science 261:45–50. http://dx.doi.org/10.1126/science.261.5117.45.
ten Brink, U.S., Hackney, R.I., Bannister, S., Stern, T.A., Makovsky, Y., 1997. Uplift of the Transantarctic Mountains and the bedrock beneath the east Antarctic ice sheet. J. Geophys. Res. 102:27603–27621. http://dx.doi.org/10.1029/97JB02483.
Tesauro, M., Kaban, M.K., Cloetingh, S.A.P.L., 2012. Global strength and elastic thickness of the lithosphere. Glob. Planet. Chang. 90–91:51–57. http://dx.doi.org/10.1016/j.gloplacha.2011.12.003.
Trey, H., Cooper, A.K., Pellis, G., della Vedova, B.D., Cochrane, G., Brancolini, G., Makris, J., 1999. Transect across the west Antarctic rift system in the Ross Sea, Antarctica. Tectonophysics 301:61–74. http://dx.doi.org/10.1016/S0040-1951(98)00155-3.
Watson, T., Nyblade, A., Wiens, D.A., Anandakrishnan, S., Benoit, M., Shore, P.J., Voigt, D., VanDecar, J., 2006. P and S velocity structure of the upper mantle beneath the Transantarctic Mountains, East Antarctic craton, and Ross Sea from travel time tomography. Geochem. Geophys. Geosyst. 7, Q07005. http://dx.doi.org/10.1029/2005GC001238.
Watts, A.B., 1978. An analysis of isostasy in the world's oceans 1. Hawaiian-emperor seamount chain. J. Geophys. Res. 83:5989–6004. http://dx.doi.org/10.1029/JB083iB12p05989.
Watts, A.B., 2001. Isostasy and Flexure of the Lithosphere. Cambridge University Press, Cambridge.
Watts, A.B., Burov, E.B., 2003. Lithospheric strength and its relationship to the elastic and seismogenic layer thickness. Earth Planet. Sci. Lett. 213:113–131. http://dx.doi.org/10.1016/S0012-821X(03)00289-9.
Watts, A.B., Fairhead, J.D., 1999. A process-oriented approach to modeling the gravity signature of continental margins. Lead. Edge 18:258–263. http://dx.doi.org/10.1190/1.1438270.
Watts, A.B., Cochran, J.R., Selzer, G., 1975. Gravity anomalies and flexure of the lithosphere: a three-dimensional study of the Great Meteor seamount, northeast Atlantic. J. Geophys. Res. 80:1391–1398. http://dx.doi.org/10.1029/JB080i011p01391.
Wessel, P., Smith, W.H.F., 1998. New, improved version of generic mapping tools released. Eos. Trans. AGU 79. http://dx.doi.org/10.1029/98EO00426 (579–579).
Wienecke, S., Braitenberg, C., Götze, H.-J., 2007. A new analytical solution estimating the flexural rigidity in the central Andes. Geophys. J. Int. 169:789–794. http://dx.doi.org/10.1111/j.1365-246X.2007.03396.x.
van Wijk, J.W., Lawrence, J.F., Driscoll, N.W., 2008. Formation of the Transantarctic Mountains related to extension of the west Antarctic Rift system. Tectonophysics 458: 117–126. http://dx.doi.org/10.1016/j.tecto.2008.03.009.
Yamasaki, T., Miura, H., Nogi, Y., 2008. Numerical modelling study on the flexural uplift of the Transantarctic Mountains. Geophys. J. Int. 174:377–390. http://dx.doi.org/10.1111/j.1365-246X.2008.03815.x.
Zuber, M.T., Bechtel, T.D., Forsyth, D.W., 1989. Effective elastic thicknesses of the lithosphere and mechanisms of isostatic compensation in Australia. J. Geophys. Res. 94: 9353. http://dx.doi.org/10.1029/JB094iB07p09353.